Clay Minerals, (2017) **52**, 351–363

Clay minerals, $\delta^{13}C$ values, pollen and non-pollen palynomorphs as palaeoenviromental and palaeoclimatic indicators in Pliocene sediments of central Anatolia, Turkey

Ş. ALI SAYIN[1,*], NURDAN YAVUZ[2] AND SERAP IÇÖZ[2]

[1] *Department of Geological Engineering, University of Aksaray, Aksaray, Turkey*
[2] *General Directorate of Mineral Research and Exploration, Ankara, Turkey*

(*Received 26 May 2017; revised 26 September 2017; Guest Associate Editor: Z. Semra Karakas*)

ABSTRACT: The Çankırı Basin is one of the largest Cenozoic basins in Central Anatolia, Turkey and contains possible economic hydrocarbon and evaporite reserves. Gypsum is the dominant mineral in the evaporite-bearing Pliocene deposits of the Çankırı Basin. In claystones, the abundance of smectite, dolomite, illite/mica and chlorite in association with minor amounts of mixed-layer chlorite-smectite, mica-vermiculite, amphibole, serpentine, quartz and feldspar together indicate an alkaline environment. Minor kaolinite is also present in some clay samples. Smectite is both detrital and authigenic. Palynological analysis revealed the existence of a mixed forest (*Pinus, Cathaya, Tsuga, Cedrus, Abies, Quercus, Ulmus, Juglans, Pterocarya, Acer, Carya, Carpinus, Fagus*) dominated by *Pinus* with a widespread herbaceous understory (Poaceae) interspersed sparsely with open areas occupied by Asteraceae. This flora reflects warm-temperate and humid climatic condition. $\delta^{13}C$ analyses have shown that the vegetation was dominated by C3 plants.

KEYWORDS: smectite, mixed-layer clays, pollen, $\delta^{13}C$ analysis, palaeoclimate, palaeoenvironment, Çankiri Basin, central Anatolia, Turkey.

The Late Tertiary Çankırı fore-arc Basin is located in Central Anatolia (Fig. 1) and lies within the İzmir–Ankara–Erzincan suture which demarcates the former position of the northern branch of the Neo-Tethyan Ocean (Kaymakç, 2000). It was formed by northward subduction of the Neo-Tethyan Ocean floor beneath the Sakarya continent (Fig. 2). During the Late Palaeocene–Early Eocene it was covered by a transgressive sea. Beginning in the Middle Eocene, mainly south-vergent thrusts developed around the Çankırı Basin. Due to the compressional regime, older units surrounding the basin thrusted over younger infills, the basin rose, shallowed up and became a continental intermontane basin. During the Late Eocene–Oligocene, terrestrial deposits and evaporites were deposited. The basin was characterized by alluvial fans during the Oligocene while evaporitic lake deposits were formed during the Late Miocene–Pliocene (Tüysüz & Dellaloğlu, 1994) (Fig. 3).

Previous work on the geology, sedimentology and economic potential of the Çankırı Basin (Gündoğan &

* E-mail: sasayin@gmail.com
This paper is one of a group published in this issue which was originally presented at the Mediterranean Clay Conference, held in Izmir, Turkey in September 2016.
https://doi.org/10.1180/claymin.2017.052.3.06

FIG. 1. Location of the Çankırı Basin, Turkey.

Helvacı, 2001; Varol *et al.*, 2002) studied basin-fill deposits of the evaporite-dominated Çankırı Basin in detail and identified the primary and secondary gypsum deposits. Three stages of evaporite development have been identified within the Çankırı Basin (Karadenizli, 2011). No detailed studies have, thus far, focused on the clay mineralogy of the sediments of the Çankırı Basin. The aim of the

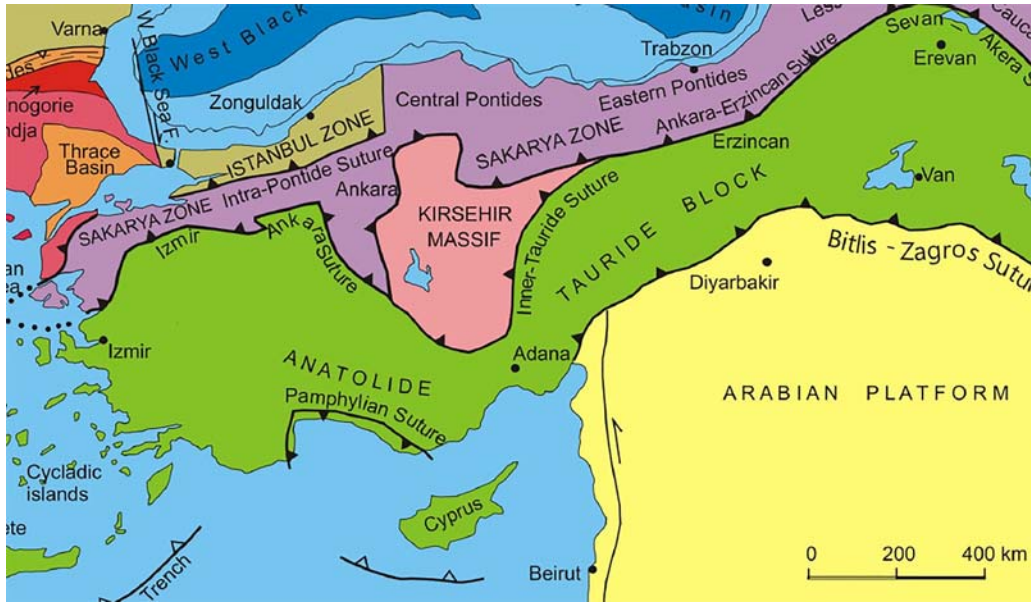

FIG. 2. Tectonic map of Turkey and the surrounding areas (Okay & Tüysüz, 1999). The omega shape of the Ankara–Erzican Suture, confining the upper boundary of the Kırşehir Massif, defines the approximate boundary with the Çankırı Basin.

https://doi.org/10.1180/claymin.2017.052.3.06 Published online by Cambridge University Press

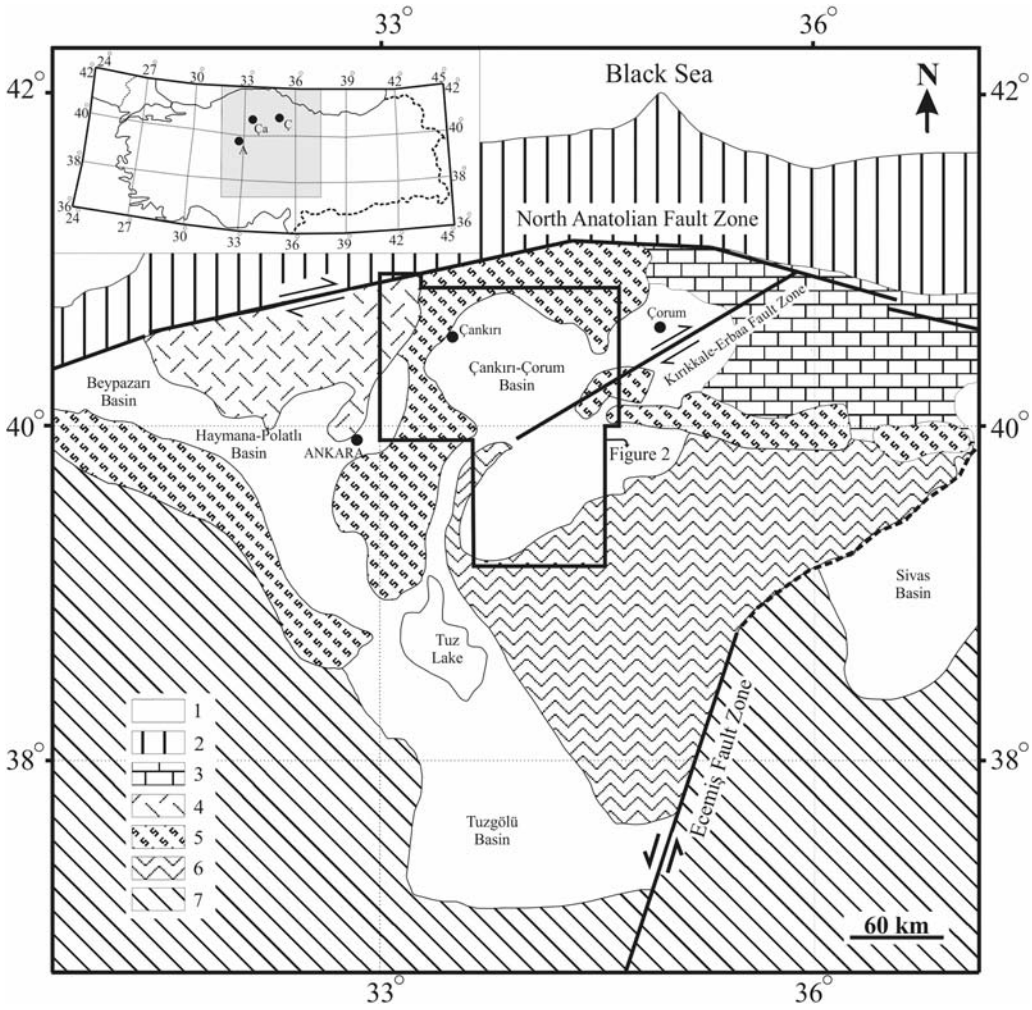

FIG. 3. Geological map of the Çankırı Basin. A: Ankara; Ça: Çankırı; Ç; Çorum (inset map of Turkey). (1) Tertiary sedimentary and evaporitic in-fills; (2) Rhodope-Pontide Block; (3) Sakarya continent; (4) Galatian Volcanic Complex; (5) Ophiolitic melange; (6) Kirşehir continent; (7) Tauride Block (Karadenizli, 2011). The solid line indicates the Çankırı-Çorum Basin.

present study was to investigate the mineralogy and palynology of the evaporite-bearing deposits within the basin to provide a better understanding of palaeoenvironmental and palaeoclimatic conditions and also to investigate modes of formation of clay minerals within the Çankırı Basin.

STRATIGRAPHY

The oldest Neogene unit in the Çankırı Basin is the Kılçak Formation of Aquitanian age. It is followed by the Altıntaş Formation of Burdigalian age, the Hançılı Formation of Burdigalian to Langhian age, the Çandır Formation possibly of Burdigalian to Serravalian age, the Bayındır Formation of Tortonian age, the Kızılırmak Formation of Messinian to Pliocene age, the Bozkır Formation of early Pliocene age and the Değim Formation of early Quaternary age (Kaymakç, 2000; Karadenizli, 2011) (Fig. 4).

The samples of the present study come from the Bozkır Formation. The evaporite-bearing Bozkır Formation, first defined by Birgili *et al.* (1975), is widespread in the Çankırı Basin with its undeformed stratification. It contains terrestrial deposits, mainly Ca sulfate-bearing

https://doi.org/10.1180/claymin.2017.052.3.06 Published online by Cambridge University Press

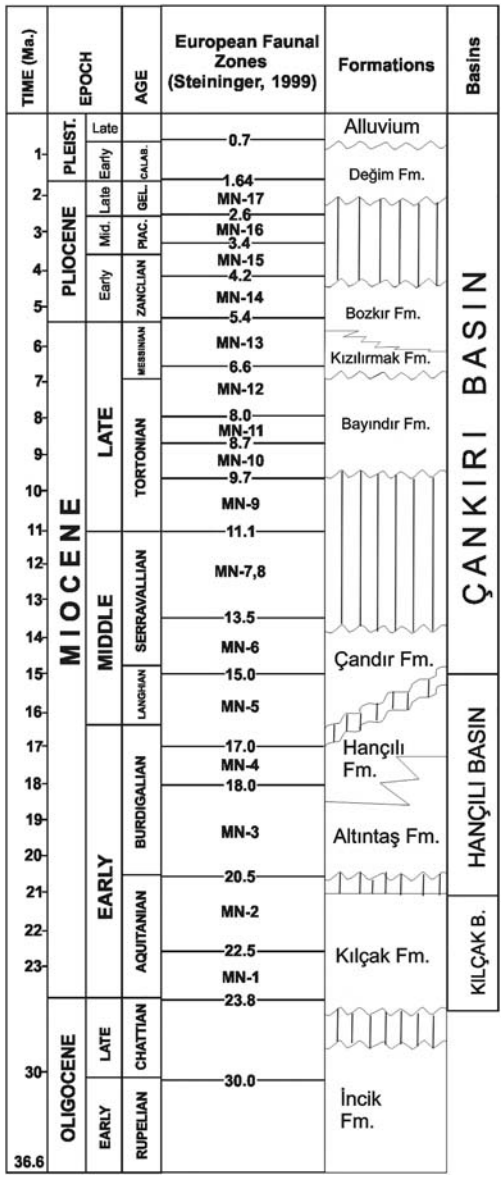

FIG. 4. Generalized stratigraphic column of the units exposed in and around the Çankırı Basin (Kaymakç, 2000).

evaporites and claystones. The Bozkır Formation is early Pliocene in age (Karadenizli *et al.*, 2004).

MATERIALS AND METHODS

The sediments of the Bozkır Formation can be divided into two parts, the lower part being represented mainly by secondary gypsum and the upper part consisting of predominantly primary gypsum in the form of selenite and gypsarenites (Varol *et al.*, 2002). This investigation focuses on the upper part of the Bozkır Formation. In the study area, close to Değim village, the stratigraphic section of the Bozkır Formation is ~100 m thick and is composed of gypsum, clayey gypsum and claystone alternations (Fig. 5). The thickness of the claystone varies between 4 and 18 m along the section. A selenite bed is present at the very bottom of the section and gypsarenites are dominant in the upper parts (Fig. 6a,b). One hundred and four samples were collected from the measured stratigraphic section for X-ray diffraction (XRD), palynological and isotopic analysis.

XRD analysis

Ninety seven whole clay samples were prepared for powder XRD analysis. The samples were crushed, ground to a particle size of <63 μm using a Retsch-BB50 machine and examined in randomly oriented mounts. The XRD analyses were carried out using a Panalytical Expert Pro diffractometer with Cu-$K\alpha$ radiation and a scanning speed of 1°2θ/min, at the mineralogical laboratories of the General Directorate of Mineral Research and Exploration (MTA), Turkey. The <2 μm clay size fractions were prepared for XRD analysis according to U.S. Geological Survey Open-File Report 01-041. Briefly, 10 g of crushed and powdered sample were dispersed in distilled water in a glass tube with 0.1 g of Calgon solution, stirred with ultrasonic probe for 5 min and allowed to settle for 3 h at room temperature. The upper 5 cm of the suspension was pipetted off and put on glass slides for drying (air-dried, oriented samples). The air-dried samples were solvated with ethylene glycol at 60°C for 2 h and then were heated at 300°C and 550°C for 2 h. Semi-quantitative mineralogical determinations of the clay samples were obtained by multiplying the intensities of the principal basal reflections of each mineral with suitable factors according to external methods developed by Gündoğdu (1982) after Brindley (1980).

SEM analysis

For microstructure investigation, four selected clay samples were examined using a field emission image scanning electron microscope (FEI Inspect F50) equipped with Energy dispersive X-ray analysis facilities (EDX, Octane Elect Plus).

https://doi.org/10.1180/claymin.2017.052.3.06 Published online by Cambridge University Press

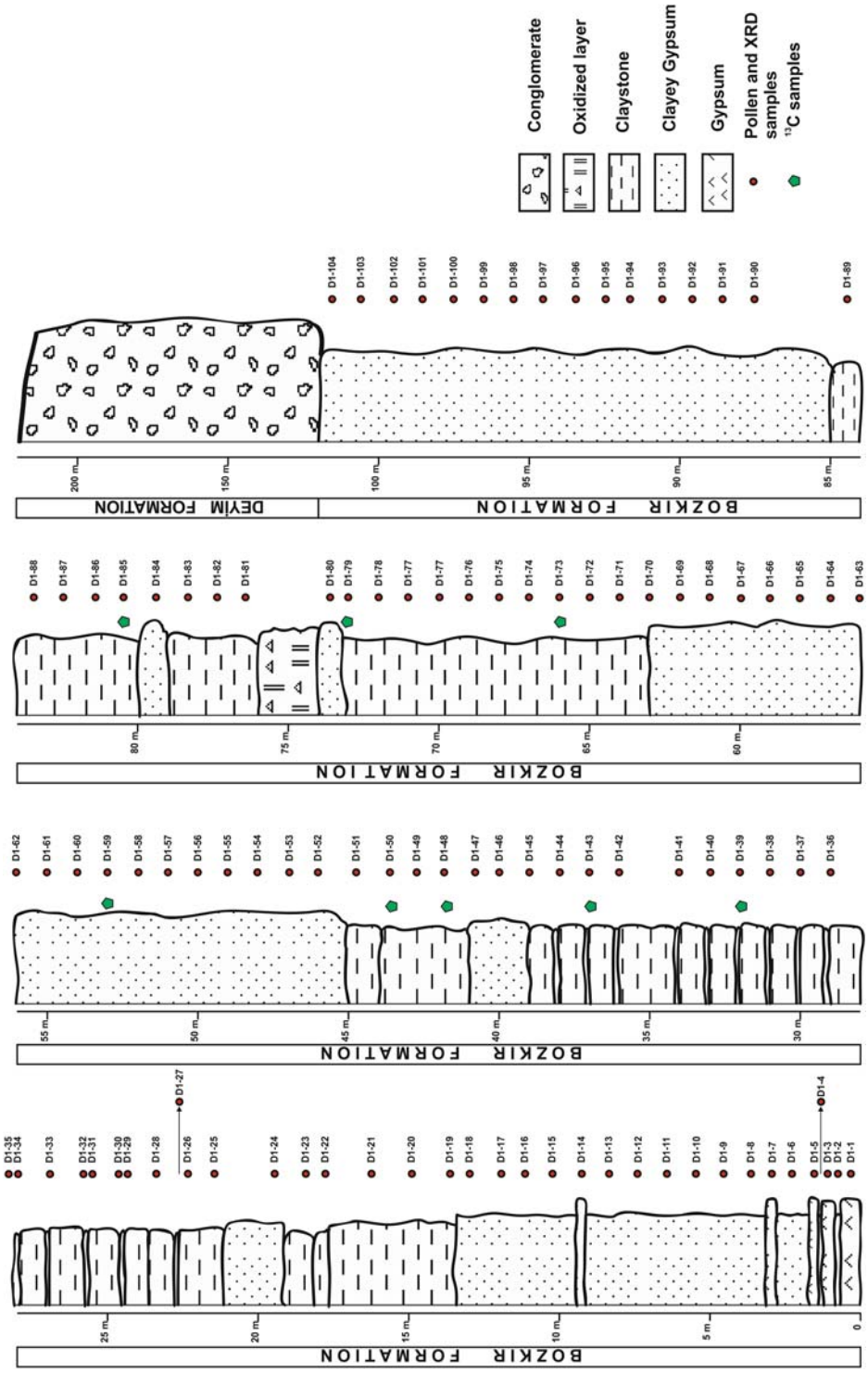

FIG. 5. The stratigraphic section of Değim.

https://doi.org/10.1180/claymin.2017.052.3.06 Published online by Cambridge University Press

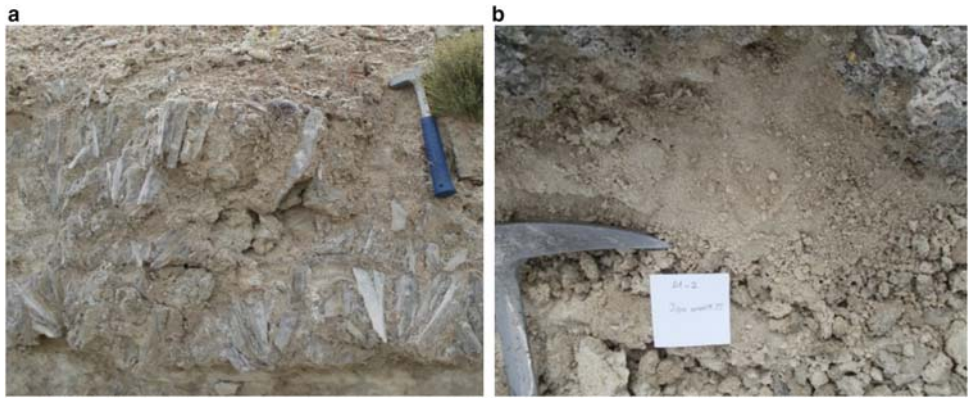

FIG. 6. (a) Selenitic gypsum within the Bozkır Formation; (b) gypsarenites within the Bozkır Formation.

Palynological analysis

Approximately 25 g of each material was processed for palynological analysis. The treatment involved cold HCl (33%) and HF (70%) to remove carbonates and silicates, and separation of the organic residue by means of $ZnCl_2$ (density 2.1–2.2 g/cm^3). The residue was sieved at 10 μm using a nylon mesh, mixed with glycerin and mounted on microscope slides. The slides were counted using a Nikon Eclipse-Ni transmitted light microscope at ×400 and ×1000 (oil immersion) magnifications to a minimum pollen sum of 200 pollen grains per sample. Fossil pollen was compared with present-day counterparts using published keys. Of the 104 samples collected, only 27 polliniferous samples allowed for quantitative analyses. The pollen results were plotted in a detailed diagram (Fig. 7). The freshwater algae (*Botryococcus*) and testate amoebae (*Arcella*) were also detected and they are the only non-pollen palynomorphs in the samples.

$\delta^{13}C$ analysis

$\delta^{13}C$ analysis of eight samples was carried out at the Environmental Isotope Laboratory at the University of Arizona, USA. The samples were measured on a continuous-flow gas-ratio mass spectrometer

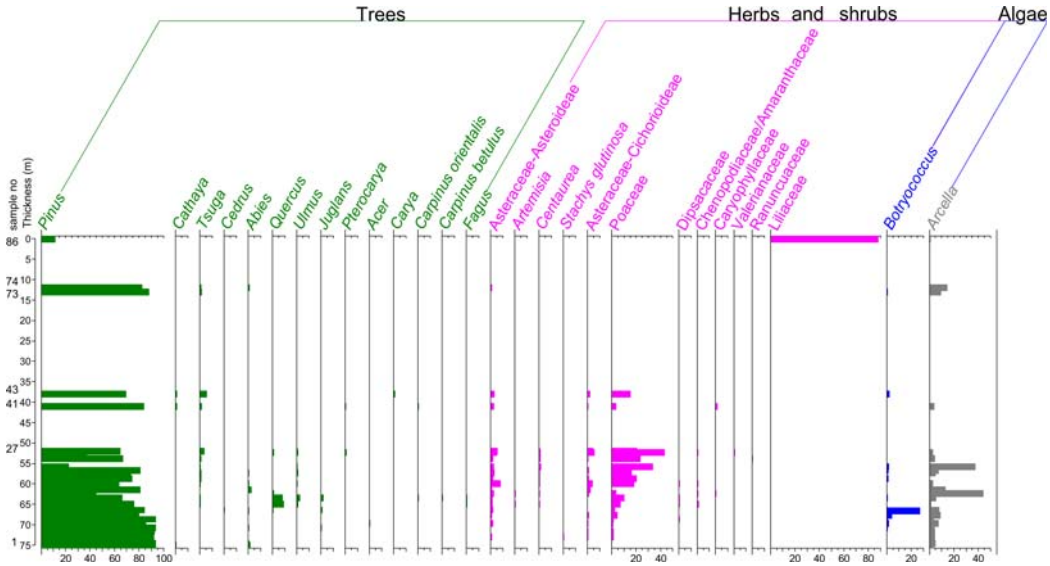

FIG. 7. Palynological diagram of the Değim section.

https://doi.org/10.1180/claymin.2017.052.3.06 Published online by Cambridge University Press

(Finnigan Delta PlusXL) coupled with an elemental analyzer. Analytical precision was better than ±0.08‰. Calibration to the VPDB standard was performed by repeated measurements of international reference standards NBS-19 and NBS-18.

RESULTS

Mineralogy

Observation under the binocular microscope showed the presence of muscovite in the clay samples. Due to difficulties in distinguishing illite from muscovite, illite-mica notation is generally used and was followed in the present study. Except for sample D1-26, smectite is the dominant clay mineral within the claystones (Table 1). Abundant illite-mica and chlorite, up to 20% and 15%, respectively, are also present in the claystones. Minor mixed-layer C-S and M-V are also observed in all samples. The assignment of peaks in mixed-layer phases followed Moore & Reynolds (1989). Thus, in the air-dried patterns, the 10.66 Å peak corresponds to mixed-layer M-V and in the ethylene glycol-solvated XRD patterns the 15.62 and 7.14 Å peaks correspond to mixed-layer C-S and the 10.65 Å peak to mixed-layer M-V. The 12.20 and 7.16 Å peaks correspond to mixed-layer C-S and in samples heated at 550°C the peaks at 11.87 Å also correspond to mixed-layer C-S (Fig. 8). Minor kaolinite is also present in certain samples. Most claystone samples contain abundant dolomite and calcite. Minor quartz and feldspar and trace amounts of serpentine and amphibole are observed in all clay samples.

The samples collected from the clayey gypsum bed contain gypsum as the predominant phase, associated with minor amounts of basanite and anhydrite. Most samples contain minor amounts of smectite, illite-mica, chlorite, mixed-layer C-S, dolomite, calcite, quartz, feldspar, serpentine and amphibole.

SEM observation

Studies by SEM of selected samples from amongst the claystones (Fig. 9) showed that detrital quartz and smectite forms small flocs (sample D1-43-SE3, Fig. 9a). Neoformation of curly smectite crystals suggests the destruction of mafic minerals, probably mica, feldspar, dolomite, amphibole or/and serpentine in authigenic systems (sample D1-43-SE2, Fig. 9b). Curly smectite crystals appear to develop on dolomite (sample D1-43-SE5, Fig. 9c). Authigenic chlorite is commonly associated with authigenic smectite. Furthermore, mixed-layer C-S was observed in many samples (*e.g.* sample D1-79-SE1, Fig. 9d); small, platy crystals, probably of kaolinite, developed on detrital smectite flocs (sample D1-79-SE4, Fig. 9e); lath-shaped primary gypsum is associated with smectite and quartz (sample D1-86-SE, Fig. 9f). Analysis by EDAX of the smectite (sample D1-79-SE4) and chlorite (sample D1-79-SE1) is shown in Fig. 10.

Palynology

The Değim pollen diagram is characterized by a predominance of *Pinus* (11–94%, Fig. 7). Other coniferous trees are represented by *Cathaya* (max. 1%), *Tsuga* (max. 5%), *Abies* (max. 2%) and *Cedrus* (max. 1%). Broad-leaved trees are represented by *Quercus* (max. 9%), *Ulmus* (max. 2%), *Carya* (max. 1%), *Pterocarya* (max. 1%), *Juglans* (max. 2%), *Acer* (<1%), *Carpinus* (max. 1%) and *Fagus* (<1%).

Among herbs and shrubs, Poaceae is well represented (maximum value 43%) while Liliaceae dominates (88%) in one sample in which it is present. Other herbs identified in smaller amounts include Asteraceae-Asteroideae (max. 8%), Asteraceae-Cichorioideae (max. 6%), Dipsacaceae (<1%), Chenopodiaceae/Amaranthaceae (max. 1%), Caryophyllaceae (max. 1%), Valerianaceae (<1%), *Centaurea* (max. 2%), Ranunculaceae (<1%) and *Artemisia* (<1%). The freshwater algae, *Botryococcus*, reaches a maximum value of 4% while amoeboid protozoa *Arcella* ranges from 1 to 15%.

$\delta^{13}C$ values

The stable carbon isotope ratio difference for a sample relative to the Pee Dee Belemnite (PDB) standard is given as:

$$\delta^{13}C(‰) = \left[\frac{(R_{sample} - RPDB)}{RPDB}\right] \times 1000$$

where R is the isotope ratio $^{13}C/^{12}C$. PDB, which has long been established as a standard for ^{13}C analysis, is based on a Cretaceous marine fossil (*Belemnitella americana*) found within the Pee Dee Formation in South Carolina (USA). This material has an anomalously high $^{13}C/^{12}C$ ratio (0.0112372), greater than nearly all other natural carbon-based materials. For convenience, it is assigned a $\delta^{13}C$ value of zero, giving almost all other naturally occurring samples

https://doi.org/10.1180/claymin.2017.052.3.06 Published online by Cambridge University Press

TABLE 1. Semi-quantitative analyses of the claystones within the Bozkır Formation (Çankırı Basin).

Sample	Sme	I-M	C-S mixed-layer	M-V mixed-layer	Kao	Chl	Qz	Fsp	Gp	Dol	Cal	Amp	Srp
D1-20	+	–	x	x		–	x	x	–	+	x	ac	x
D1-23	–	– x	–	x		– x	x	x	– x	+		ac	ac
D1-25	+	–	x	x	x	–	x	x	–	– x	x	ac	x
D1-26		+	–	x		– x	x	x	– x	+	x	ac	x
D1-27	+ x	– x	x			–	x		– x	+ x		ac	x
D1-28	+	– x	x	ac	x	–	x	x	–	+		x	ac
D1-36	+ –	– x	ac	ac	x	x	x	ac	–	+	–	ac	ac
D1-39	+ –	x		ac	x	–x	x	x	–	–	x	x	x
D1-41	+ x	–	x	ac		–	x	x	– x	– x	x	ac	x
D1-43	+ x	–	x	ac	x	–	x	x	x	+	–		ac
D1-49	+ –	–	x	ac	x	–	x	x	–	+	x	x	ac
D1-51	+ x	–	x	ac	x	– x	x	x	–	– x	–	ac	ac
D1-72	+	–	x			–	x	x	– x	– x	– x		ac
D1-74	+	–	–	x		–	x	x	– x	–	–	ac	x
D1-76	+ x	–	x	x	x	–	x	x	–	x	–		x
D1-79	+ x	–	x	ac	x	–	x	x	–	x	– x	x	x
D1-86	+	–	x	ac		–	x	x	–	–	x	x	x
D1-88	+ x	–	x	x		–	x	x	–	– x		x	ac

[(+) ~20 wt.%, (–) ~10 wt.%, (x) ~5 wt.%, (ac) accessory. Sme = smectite, Chl = chlorite, I-M = illite-mica, Kao = kaolinite, C-S mixed-layer = mixed-layer chlorite-smectite, M-V mixed-layer = mixed-layer mica-vermiculite, Gp = gypsum, Dol = dolomite, Cal = calcite, Qz = quartz, Fsp = feldspar, Amp = amphibole, Srp = serpentine].

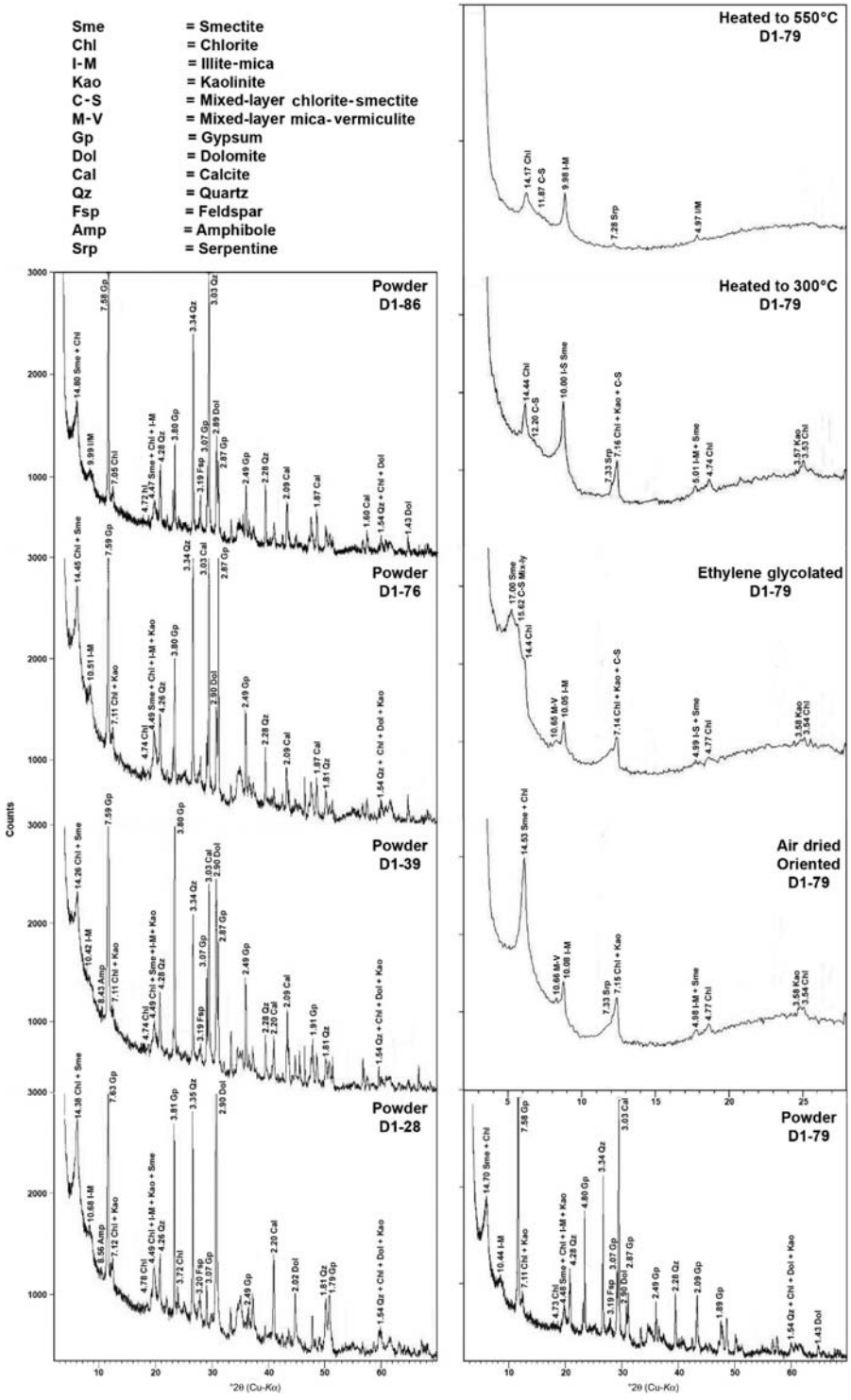

FIG. 8. XRD patterns of selected samples from the claystones of the Bozkır Formation.

https://doi.org/10.1180/claymin.2017.052.3.06 Published online by Cambridge University Press

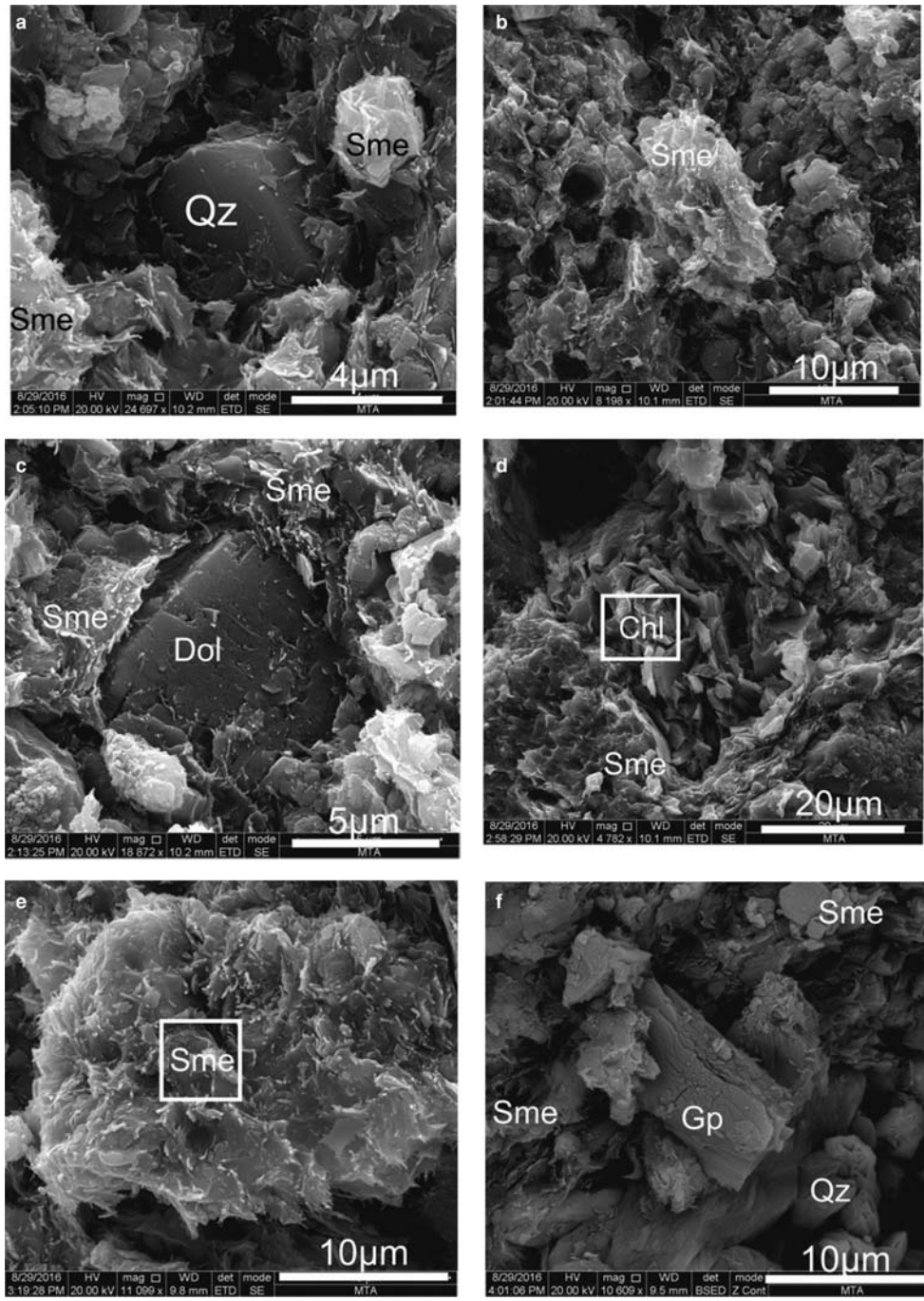

FIG. 9. SEM images of clays: (a) detrital smectite crystals (sample D1-43-SE3); (b) curly smectite crystals in sample D1-43-SE2; (c) smectite crystal developed on dolomite crystal (sample D1-43 SE5); (d) authigenic platy chlorite and curly smectite crystals (sample D1-79-SE1); (e) slightly curled smectite crystals forming a large floc (sample D1-79-SE4). Small platy crystals (probably of kaolinite) are draped on the smectite floc; (f) lath-shaped gypsum crystal associated with detrital smectite and quartz (sample D1-86-SE2). Sme: smectite. Chl: chlorite Qz: quartz. Dol: dolomite. Gp: gypsum.

https://doi.org/10.1180/claymin.2017.052.3.06 Published online by Cambridge University Press

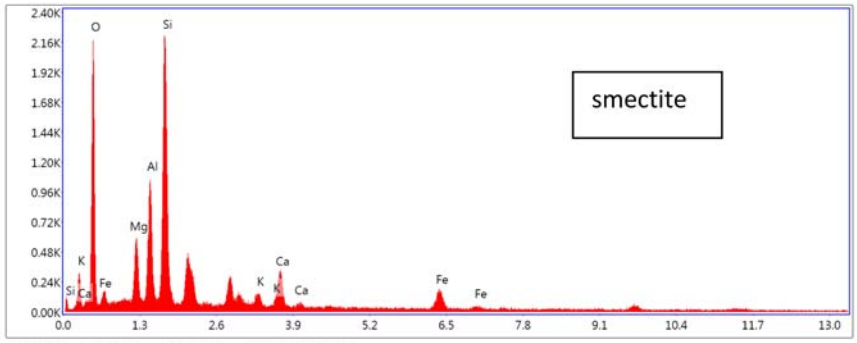

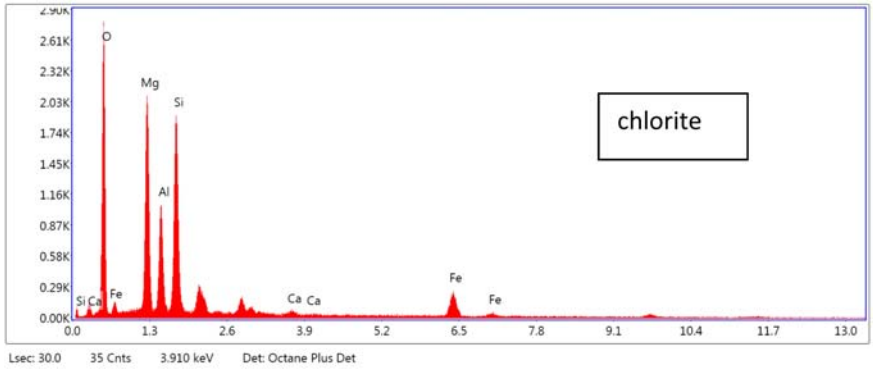

Element	Wt %	Atomic %	Net Int.	Error %	K_{ratio}	Z	R	A	F
O K	49.23	65.12	396.98	8.74	0.1673	1.0605	0.9672	0.3204	1.0000
MgK	5.39	4.69	114.08	9.09	0.0264	0.9813	1.0015	0.4953	1.0086
AlK	9.65	7.57	238.16	6.94	0.0549	0.9453	1.0088	0.5949	1.0106
SiK	21.47	16.17	566.93	5.58	0.1338	0.9662	1.0156	0.6422	1.0046
K K	1.56	0.85	34.42	13.95	0.0131	0.8965	1.0445	0.9052	1.0350
CaK	5.29	2.80	100.90	6.69	0.0463	0.9130	1.0493	0.9324	1.0284
FeK	7.41	2.81	70.98	8.13	0.0643	0.8145	1.0702	0.9991	1.0665

Element	Wt %	Atomic %	Net Int.	Error %	K_{ratio}	Z	R	A	F
O K	44.11	58.65	514.00	7.73	0.1913	1.0624	0.9682	0.4083	1.0000
MgK	18.57	16.25	475.66	6.64	0.0975	0.9830	1.0024	0.5307	1.0064
AlK	9.97	7.86	238.13	7.81	0.0486	0.9469	1.0097	0.5108	1.0076
SiK	17.82	13.50	474.27	6.41	0.0992	0.9679	1.0165	0.5728	1.0035
CaK	0.77	0.41	16.63	22.10	0.0068	0.9145	1.0500	0.9308	1.0362
FeK	8.76	3.34	95.54	6.06	0.0767	0.8157	1.0707	1.0044	1.0685

FIG. 10. EDAX analysis of smectite (sample D1-79-SE4) (upper panel of data) and chlorite (sample D1-79-SE1) (lower panel of data).

https://doi.org/10.1180/claymin.2017.052.3.06 Published online by Cambridge University Press

negative delta values (http://siel.uga.edu/stable-isotope-overview).

The $\delta^{13}C$ values of the samples are listed in Table 2. The $\delta^{13}C$ values range between −24.5‰ and −25.7‰ with a mean of −25.1‰. The minor fluctuations in the $\delta^{13}C$ values indicate that vegetation remained virtually unchanged during deposition.

DISCUSSION

XRD analysis and texture of clays

Smectite is the predominant clay mineral within the clay beds of the Bozkır formation. Illite-mica, kaolinite, mixed-layer C-S and M-V are also present. Both detrital and neoformed smectite (reworked) are common within the claystones (Fig. 8). The neoformation of smectite and mixed-layer clay minerals is probably related to the destruction of mica, feldspar, dolomite, amphibole and serpentine minerals in authigenic systems, with hydrogen metasomatism being the main mechanism responsible for the destruction (Hemley & Jones, 1964; Sayın, 1984). The H^+ ions from the altering solution replace Fe, Mg, Ca, Na, K, Al and Si from the clay minerals. Very small platy crystals (probably kaolinite) appear to have been formed from the *in situ* breakdown of the detrital smectite. In the case of a H^+ ion-dominated altering solution, smectite is converted to kaolinite (Kukovsky, 1969; Keller, 1976; Sayın, 1984, 2007, 2015). In this context, warm and humid conditions accelerate the dissolution of smectite for the development of kaolinite crystals (Kemp *et al*., 2016 and references therein). In addition, authigenic smectite and mixed-layer C-S and M-V are the first clay minerals to form at the beginning of H metasomatism of sediments at the expense of mica, feldspar, dolomite, amphibole and serpentine as a result of a dissolution-precipitation mechanism.

TABLE 2. $\delta^{13}C$ data for Değim samples, central Anatolia.

Lab number[a]	Material dated	$\delta^{13}C$ (‰)
D1-39	Bulk organic sediment	−25.2
D1-43	Bulk organic sediment	−24.5
D1-48	Bulk organic sediment	−24.9
D1-50	Bulk organic sediment	−24.7
D1-59	Bulk organic sediment	−25.3
D1-73	Bulk organic sediment	−25.7
D1-79	Bulk organic sediment	−25.5
D1-85	Bulk organic sediment	−25.7

[a]Sample number assigned at the radiocarbon laboratory (Environmental Isotope Laboratory at the University of Arizona, USA).

Palynology

The regular occurrence and abundance of *Pinus*, the moderate presence of altitudinal elements (*Cathaya, Cedrus, Abies*) and broadleaved trees (*Quercus, Ulmus, Juglans, Pterocarya, Acer, Carya, Carpinus, Fagus*) and the scarcity of herbs, except Poaceae, are characteristic of the vegetation at the time of sediment deposition. This palynoflora reflects the presence of a mixed evergreen and deciduous forest. The open areas within this forest were covered mainly by Poaceae and lesser amounts of Asteraceae, Dipsacaceae, Chenopodiaceae, Caryophyllaceae and Ranunculaceae. The persistent presence of amoeboid protozoa *Arcella*, together with freshwater algae *Botryococcus*, indicate the presence of freshwater at the time of deposition.

Wick (2000) showed that terrestrial plant ecosystems responded to environmental changes and minor climatic fluctuations are significantly more distinct in the pollen record than in other proxy data. Thus the consistent presence of mesothermic plants within the studied samples indicate a humid, warm temperate climate.

Isotope analysis

The differences in the $^{13}C/^{12}C$ ratio of terrestrial plants is the result of differences in the metabolic pathways during synthesis of the plant material. The range in $\delta^{13}C$ for C3 plants is from −33 to −22‰ and for C4 plants from −20 to −10‰ (Bender, 1971). The $\delta^{13}C$ values of the samples studied indicate that vegetation was dominated by C3 plants during their time of formation.

CONCLUSIONS

The upper part of the studied section within the Bozkır Formation comprises the alternation of gypsarenites and claystones. Smectite and illite-mica are the predominant clay minerals within the claystones, with mixed-layer C-S, M-V and kaolinite being present in minor amounts. Gypsum, dolomite, calcite and chlorite are associated with small amounts of quartz, feldspar, amphibole and serpentine within the claystones. The smectites were both detrital and authigenic, with the latter derived *via* a mechanism of both dissolution and precipitation within the claystones. The palynoloflora

https://doi.org/10.1180/claymin.2017.052.3.06 Published online by Cambridge University Press

identified indicate the presence of a mixed coniferous forest during the early Pliocene. The reconstructed vegetation points to a warm-temperate climate for the Çankırı Basin at the time of deposition.

ACKNOWLEDGEMENTS

The authors are grateful to Şükrü Sinan Demirer (General Directorate of Mineral Research and Exploration, Ankara) and Ertan Öner (IT officer of Aldridge Minerals Inc.) for drafting most of the figures. The authors also acknowledge Ufuk Kibar for the SEM studies.

REFERENCES

Bender M.M. (1971) Variations in the $^{13}C/^{12}C$ ratios of plants in relation to the pathway of photosynthetic carbon dioxide fixation. *Phytochemistry*, **10**, 1239–1243.

Birgili Ş., Yoldaş R. & Ünalan G. (1975) Çankırı-Çorum Havzası'nın jeolojisi ve petrol olanakları. Maden Tetkik ve Arama Genel Müdürlüğü Rapor No.5621, 106 pp.

Brindley G.W. (1980) Quantitative X-ray analysis of clays. Pp. 441–458 in: *Crystal Structure of Clay Minerals and Their X-ray Identification* (G.W. Brindley & G. Brown, editors). Monograph **5**, Mineralogical Society, London.

Gündoğan İ. & Helvacı C. (2001) Sedimentological and petrographical aspects of Upper Miocene evaporites in the Beypazarı and Çankırı–Çorum Basins, Central Anatolia, Turkey. *International Geology Review*, **43**, 818–829.

Gündoğdu M.N. (1982) *Geological, mineralogical and geochemical investigation of the Bigadiç Neogene Sedimentary Basin*. PhD thesis, Hacettepe University, Ankara, Turkey.

Hemley J.J. & Jones W.R. (1964) Chemical aspects of hydrothermal alteration with emphasis on the hydrogene metasomatism. *Economic Geology*, **59**, 538–569.

Karadenizli L. (2011) Oligocene to Pliocene palaeogeographic evolution of the Çankırı–Çorum Basin, central Anatolia, Turkey. *Sedimentary Geology*, **237**, 1–29.

Karadenizli L., Saraç G., Şen Ş., Seyitoğlu G., Antoine P. O., Kazancı N., Varol B., Alçiçek C., Gül A., Ertan H. *et al.* (2004) Çankırı-Çorum Havzasının batı ve güney kesiminin memeli fosillere dayalı Oligo-Miyosen biyostratigrafisi ve dolgulanma evrimi. Maden Tetkik ve Arama Genel Müdürlüğü Raporu No.107006, 199 pp.

Kaymakç N. (2000) *Tectono-stratigraphical evolution of the Çankırı Basin (Central Anatolia, Turkey)*. PhD thesis, Geologica Ultraiectina, No. 190. Utrecht University, The Netherlands, 247 pp.

Keller W.D. (1976) Scan electron micrographs of kaolin collected from diverse origin – III. Influence of parent material on flint clays and flint-like clays. *Clays Clay Minerals*, **24**, 262–264.

Kemp S.J., Ellis M.A., Mounteney I. & Kender S. (2016) Palaeoclimatic implications of high-resolution clay mineral assemblages preceding and across the onset of the Palaeocene–Eocene Thermal Maximum, North Sea Basin. *Clay Minerals*, **51**, 793–813.

Kukovsky E.G. (1969) Alteration process in clay minerals. *Clay Minerals*, **8**, 234–237.

Moore D.M. & Reynolds Jr, R.C. (1989) *X-ray Diffraction and the Identification and Analysis of Clay Minerals*. Oxford University Press, Oxford, UK, 332 pp.

Okay A. & Tüysüz O. (1999) Tethyan sutures of northern Turkey. Pp. 475–515 in: *The Mediterranean Basins*: Tertiary Extension within the Alpine Orogen (B. Durand, L. Jolivet, F. Horváth & M. Séranne, editors). Special Publication **156**, Geological Society, London.

Sayın S.A. (1984) *The geology, mineralogy, geochemistry and orgin of the Yeniçağa Kaolinite Deposits and other similar deposits in Western Turkey.* PhD thesis, University of London, London, UK.

Sayın S.A. (2007) Origin of kaolin deposits: evidence from the Hisarcık (Emet-Kütahya) kaolin deposits, western Turkey. *Turkish Journal of Earth Science*, **16**, 77–96.

Sayın S.A. (2015) Quartz-mica schist and gneiss hosted clay deposits within the Yenipazar (Yozgat, Central Anatolia) volcanogenic massive sulphide ore. *Turkish Journal of Earth Science*, **24**, 1–21.

Steininger R. (1999) Chronostratigraphy, geochronology and biochronology of the Miocene "European Land Mammal Mega-Zones (ELMNZ)" and the Miocene "Mammal Zones (MN-Zones)". Pp. 9–24 in: *The Miocene Land Mammals of Europe* (G.E. Rössner & K. Heissing, editors). Verlag Dr. Freidrich Pfeil, Munich, Germany, 515 pp.

Tüysüz O. & Dellaloğlu A.A. (1994) Palaeogeographic evolution of the Çankırı Basin and surroundings, Cental Anatolia, Türkiye 10. Petrol Kongresi Bildiriler Kitabı, pp. 56–76.

Varol B., Araz H., Karadenizli L., Kazancı N., Seyitoğlu G. & Şen Ş. (2002) Sedimentology of the Miocene evaporitic succession in the north of Çankırı–Çorum Basin, Central Anatolia, Turkey. *Carbonates Evaporites*, **12**, 197–209.

Wick L. (2000) Vegetational response to climatic changes recorded in Swiss Late Glacial lake sediments. *Palaeogeography Palaeoclimatology Palaeoecology*, **159**, 231–250.